Research article

NMR IN BIOMEDICINE

Received: 30 August 2013, Revised: 29 August 2014, Accepted: 29 August 2014, Published online in Wiley Online Library

(wileyonlinelibrary.com) DOI: 10.1002/nbm.3220

Dynamic contrast-enhanced MRI in mouse tumors at 11.7T: comparison of three contrast agents with different molecular weights to assess the early effects of combretastatin A4

A.-C. Fruytier[a], J. Magat[a], M.-A. Neveu[a], O. Karroum[a], C. Bouzin[b], O. Feron[b], B. Jordan[a], G. O. Cron[c,d] and B. Gallez[a]*

Dynamic contrast-enhanced (DCE)-MRI is useful to assess the early effects of drugs acting on tumor vasculature, namely anti-angiogenic and vascular disrupting agents. Ultra-high-field MRI allows higher-resolution scanning for DCE-MRI while maintaining an adequate signal-to-noise ratio. However, increases in susceptibility effects, combined with decreases in longitudinal relaxivity of gadolinium-based contrast agents (GdCAs), make DCE-MRI more challenging at high field. The aim of this work was to explore the feasibility of using DCE-MRI at 11.7 T to assess the tumor hemodynamics of mice. Three GdCAs possessing different molecular weights (gadoterate: 560 Da, 0.29 mmol Gd/kg; p846: 3.5 kDa, 0.10 mmol Gd/kg; and p792: 6.47 kDa, 0.15 mmol Gd/kg) were compared to see the influence of the molecular weight in the highlight of the biologic effects induced by combretastatin A4 (CA4).

Mice bearing transplantable liver tumor (TLT) hepatocarcinoma were divided into two groups ($n = 5$–6 per group and per GdCA): a treated group receiving 100 mg/kg CA4, and a control group receiving vehicle. The mice were imaged at 11.7 T with a T_1-weighted FLASH sequence 2 h after the treatment. Individual arterial input functions (AIFs) were computed using phase imaging. These AIFs were used in the Extended Tofts Model to determine K^{trans} and v_p values. A separate immunohistochemistry study was performed to assess the vascular perfusion and the vascular density.

Phase imaging was used successfully to measure the AIF for the three GdCAs. In control groups, an inverse relationship between the molecular weight of the GdCA and K^{trans} and v_p values was observed. K^{trans} was significantly decreased in the treated group compared with the control group for each GdCA.

DCE-MRI at 11.7 T is feasible to assess tumor hemodynamics in mice. With K^{trans}, the three GdCAs were able to track the early vascular effects induced by CA4 treatment.

Additional supporting information maybe found in the online version of this article at the publisher's web site.

Keywords: DCE-MRI; Gd chelate-based contrast agents; animal model study; vascular disrupting agents; combretastatin A4; gadoterate, p846, p792

INTRODUCTION

Functional tumor imaging techniques provide quantitative biomarkers which can predict the success of therapy earlier than morphologic imaging (1). Such biomarkers are also helpful for assessment of new drugs and the therapeutic management of patients (2). Dynamic contrast-enhanced (DCE)-MRI allows non invasive investigation of tumor hemodynamics and estimation of physiologically relevant parameters including blood flow, vessel permeability, vascular and interstitial volume fractions (3). DCE-MRI is currently used in early-phase clinical trials of anti-angiogenic and more recently vascular disrupting agents (VDAs)

* *Correspondence to: Prof. B. Gallez, LDRI/REMA, Avenue Mounier 73.08, B-1200 Brussels, Belgium.*
E-mail: bernard.gallez@uclouvain.be

a *A.-C. Fruytier, J. Magat, M.-A. Neveu, O. Karroum, B. Jordan, B. Gallez*
Biomedical Magnetic Resonance Research Group, Louvain Drug Research Institute, Université catholique de Louvain, Brussels, Belgium

b *C. Bouzin, O. Feron*
Institut de Recherche Expérimentale et Clinique, Pole of Pharmacology, Angiogenesis and Cancer Research Laboratory, Université catholique de Louvain, Brussels, Belgium

c *G. O. Cron*
Ottawa Hospital Research Institute, Ottawa, Canada

d *G. O. Cron*
University of Ottawa Faculty of Medicine, Ottawa, Canada

Abbreviations used: *GdCA, gadolinium-based contrast agent; CA4, combretastatin A4; CA4P, combretastatin A4 phosphate; FLASH, fast low angle shot sequence; AIF, arterial input function; MW, molecular weight; ETM, Extended Tofts Model; DCE-MRI, dynamic contrast-enhanced-MRI; VDAs, vascular disrupting agents; K^{trans}, volume transfer constant between blood plasma and extravascular extracellular space; EES, extravascular extracellular space; RMSE, Root mean squared error; v_p, blood plasma volume per unit volume of tissue; TLT, transplantable liver tumor; DMSO, dimethylsulfoxyde; ROI, region of interest; F_p, blood plasma flow per unit volume of tissue; PS, permeability surface area product; 2CXM, two-compartment exchange model; TMR, tumor-to-muscle ratio; SNR, signal-to-noise ratio.*

(4). Unlike anti-angiogenic agents, which prevent the development of new blood vessels, VDAs target the established tumor vasculature leading to secondary extensive tumor necrosis (5). Combretastatin A4 (CA4) is a VDA acting as a tubulin-binding agent, leading to a destabilization of the tubulin polymers of the cytoskeleton of proliferating endothelial cells. It causes endothelial-cell shape changes and an increase in vascular permeability. Although the mechanisms of action of CA4 have not yet been completely elucidated, the increase in vascular permeability is a likely trigger for blood flow shutdown via development of tissue edema, followed by an increase in blood viscosity and/or an increase in interstitial fluid pressure (5,6). The water-soluble prodrug Combretastatin-A4 phosphate (CA4P) has recently been investigated in Phase II clinical trials in combination with chemotherapy (7) and/or with anti-angiogenic treatment (8) in solid cancers. Using DCE-MRI, decreases in the volume transfer constant between blood plasma and extravascular extracellular space (K^{trans}) and the blood plasma volume per unit volume of tissue (v_p) have been shown to be relevant markers of CA4P efficacy (9,10).

The purpose of the present work was twofold. The first goal was to show the feasibility of applying DCE-MRI at ultra-high-field (11.7 T) to provide estimates of tumor hemodynamics in mice. DCE-MRI at such high fields is challenging owing to increased susceptibility effects and decreased longitudinal relaxivity (r1) of GdCA. The r1 decrease is relatively small for commercially available extracellular agents but more marked for molecules with protein binding or with slow rotational motion (11). Susceptibility effects are particularly problematic for estimation of the arterial input function (AIF). Indeed, we showed recently that major T_2* effects in blood vessels lead to an undesirable dip in arterial magnitude signal at early time points after gadoterate meglumine injection (T_1-weighted images) (12).

The second purpose of this work was to establish the respective value of different GdCA for monitoring the effect of CA4. One of the main differences between the various types of GdCA is molecular weight (MW), which affects trans-capillary permeability (13). That permeability has a critical influence on the physiological interpretation of K^{trans}: higher permeability makes K^{trans} more reflective of blood flow, whereas lower permeability makes K^{trans} more reflective of vascular permeability (14). Previous studies have shown that the size of the GdCA may affect the measured values of K^{trans} and v_p (15,16). Given that VDAs are known to induce early tumor blood flow decrease and vascular permeability increase, the choice of contrast agent may have a significant impact on the way in which DCE-MRI tracks these two effects.

In the present study, we first established the feasibility of using DCE-MRI at 11.7 T in murine tumors using three different GdCAs differing in MW (gadoterate, p846 and p792). Phase imaging was used to measure the AIF in iliac arteries/veins. We then compared the respective value of the three GdCAs for monitoring the early effects of CA4 on the hemodynamic parameters K^{trans} and v_p. A separate immunohistochemistry study was also conducted to better understand K^{trans} and v_p changes induced by CA4.

EXPERIMENTAL

Animals

Transplantable liver tumors (TLT hepatocarcinoma (17); ascites; about 8.10^5 cells) were induced intramuscularly into the right rear leg (gastrocnemius muscle) of 5-week-old male NMRI mice (Janvier Labs, Le Genest St Isle, France). When the tumours reached 8 ± 0.5 mm diameter, mice were divided into two groups per GdCA (n = 5–6): one untreated control group receiving only vehicle [dimethylsulfoxyde (DMSO); Invitrogen, Merelbeke, Belgium] and one treated group receiving CA4 [100 mg/kg (18), intraperitoneal injection; Sigma-Aldrich, Diegem, Belgium]. MRI examination was carried out at 2 h after treatment. Animals were anesthetized by isoflurane inhalation (3% for induction and 1.5% for maintenance, mixed with air). A 24-G catheter was inserted in the caudal vein of mice for GdCA injection. Respiration rate and body temperature were monitored. Experiments were performed in accordance to national animal care regulations with the approval of local Ethics Board 2010/UCL/MD/01.

Data acquisition

All experiments were performed on a 11.7 T Biospec MRI (Bruker, Ettlingen, Germany). A quadrature whole body coil was used for radiofrequency transmission and reception (inner diameter = 40 mm, length = 10 cm). Prior to the DCE-MRI experiment, anatomical images were acquired using a T_2-weighted axial turbo spin-echo RARE sequence (TR = 2500.0 ms; TE = 33.0 ms; RARE factor = 8). Two transverse 1-mm-thick slices were selected (tumor and iliac arteries/veins). For DCE-MRI, T_1-weighted gradient echo images were obtained with a fast low angle shot sequence (FLASH) with the following parameters: TE = 2.074 ms, TR = 15.000 ms, flip angle = 40.0°, field of view = 40 mm, matrix = 128 × 64, zero-fill acceleration factor = 1.4 and spatial resolution = 0.312 mm/pixel-0.625 mm/pixel.

A first set of 400 scans with a temporal resolution of 1.19 s was acquired, with GdCA manually administered intravenously after the 20th scan over 2–3 s (number of averages = 1). Afterwards, a slower DCE data set was acquired with a temporal resolution of 10.1 s to monitor the washout of the contrast material from the tumor for about 1 h (300 images; number of averages = 10). A proton density weighted image was acquired before T_1-weighted sequences with the following parameters: TE = 2.074 ms, TR = 3500.000 ms, flip angle = 40.0°, field of view = 40 mm, matrix = 128 × 64, spatial resolution = 0.312 mm/pixel-0.625 mm/pixel.

Contrast agents

All GdCAs were kindly provided by Guerbet (Aulnay-sous-Bois, France).

Gadoterate meglumine (Gd-DOTA; Dotarem®) is a small gadolinium chelate clinically available, known as a non-specific agent. It leaves the vascular space and diffuses rapidly into the interstitium.

P846 is a low diffusion agent, a class of blood pool agents characterized by a reduced extravasation through the endothelium and a rapid renal excretion. It is constituted by a macrocyclic 3-armed gadolinium chelate (19,20).

P792 is a rapid-clearance blood-pool agent, with limited diffusion across normal endothelium and clearance equivalent to the glomerular filtration rate (21). It is a monogadolinated macrocyclic complex with a Gd-DOTA core substituted by hydrophilic bulky groups (22).

The doses were 0.29, 0.10 and 0.15 mmol Gd/kg for gadoterate meglumine, p846 and p792 respectively, corresponding to an injected volume of ~20, ~35 and ~150 µl of solution. The doses chosen were based on the tumor-to-muscle ratio (TMR) evaluated in a previous dose escalation study (data not shown). We

selected doses with a TMR superior to 2. No delay in the maximum of enhancement was observed for the selected doses compared with lower doses. R1 relaxivities at 11.7 T were established at the University of Mons (in collaboration with Professor R.N. Muller). The characteristics of the three GdCAs are summarized in Table 1 (23,24).

Data analysis

Magnitude and phase MRI data were analyzed using in-house software written in Matlab (The Mathworks, Natick, MA, USA).

AIF

The AIF was acquired using phase imaging as previously described for gadoterate (12). More details on AIF measurement by phase imaging are available in the Supplementary Data.

The concentration curve for plasma $C_p(t)$ was then fitted by a bi-exponential model (25):

$$C_p(t) = \begin{cases} 0 & t < t_1 \\ D \cdot \sum_{i=1}^{2} a_i \cdot \exp(-m_i t) & t \geq t_1 \end{cases} \quad [1]$$

using a Levenberg–Marquardt algorithm.

Here, t_1 is the arrival time (time corresponding to the maximum in the C_p curve), D is the bolus dose of GdCA. The equation is characterized by one fast and one slow exponential component, each described by two parameters: a_1 and m_1 which represent the amplitude and decay rate, respectively, of the distribution of the GdCA and a_2 and m_2 which correspond to the excretion of the GdCA. The bi-exponential model was applied for gadoterate and p846, whereas, plasmatic curves of p792 were fitted by a mono-exponential function (26), namely a_2 and m_2 equal 0. The a_i and m_i values were further used as input to the ETM (27).

Tumor kinetics

A global region of interest (ROI) was manually delineated to cover the entire tumor area (using the T_2-weighted anatomical images as reference).

Table 1. Characteristics of the three contrast agents

	Gadoterate	P846	P792
Molecular weight (kDa)	0.56	3.50	6.47
Size (nm)	1.0	4.0	5.0
Dose (mmol/kg)	0.29	0.10	0.15
R1 relaxivity ($mM^{-1}.s^{-1}$)			
at 1.5T[a]	3.5	32	27
at 3.0T[a]	3.4	24	12
at 4.7T[a]	3.3	15	7
at 7.0T[a]	3.0	11	5
at 11. T[b]	2.7	6	3

[a]37 °C, in 4% human serum albumin (Guerbet data).
[b]37°C, in water.

The signal intensity obtained from the FLASH sequence is (28):

$$S = S_0 \frac{\sin\alpha \cdot \left(1 - \exp^{\frac{-TR}{T1}}\right)}{\left(1 - \cos\alpha \cdot \exp^{\frac{-TR}{T1}}\right)} \cdot \exp\left(-\frac{TE}{T_2^*}\right) \quad [2]$$

where S_0 is a scaling factor comprising proton density and instrumental factors and is determined by the proton density sequence, α is the flip angle, TR is the repetition time, and TE is the echo time. Signal dependence on T_2^* was neglected as a result of the short echo time (TE = 2.074 ms) (29). In a tumor, the relationship between relaxation rate (1/T1) and GdCA concentration can be predicted by the Solomon–Bloembergen equation (28)

$$\frac{1}{T_1} = \frac{1}{T_{10}} + r_1 \cdot C(t), \quad [3]$$

where r1 is the longitudinal relaxivity of the GdCA at 11.7 T, T_{10} is the longitudinal relaxation time in the absence of the GdCA, C(t) is the concentration of GdCA in tissue.

The pharmacokinetic parameters were computed using a two compartmental model, the Extended Tofts Model (27). This model takes into account the contribution of the vascular compartment, which is not negligible in tumors.

$$C_t(t) = v_p \cdot C_p(t) + K^{trans} \int_0^t C_p(\tau) e^{-k_{ep}(t-\tau)} d\tau \quad [4]$$

Using the amplitude and time constants individually defined, the measured tissue concentration time course of pixels was individually fitted to the ETM using a Levenberg–Marquardt nonlinear least-squares procedure.

$$C_t(t) = K^{trans} \cdot D \cdot \sum_{i=1}^{2} a_i \frac{\exp(-k_{ep}t) - \exp(-m_i t)}{m_i - k_{ep}} + v_p \cdot D \cdot \sum_{i=1}^{2} a_i \cdot \exp(-m_i t) \quad [5]$$

where K^{trans} is the volume transfer constant between blood plasma and extravascular extracellular space (EES) [min^{-1}], v_p is the blood plasma volume per unit volume of tissue, and k_{ep} is the rate constant between EES and blood plasma [min^{-1}] (30). Some pixels provide nonphysiological values of K^{trans} ($K^{trans} < 0$, $K^{trans} > 1\ min^{-1}$) and/or v_p ($v_p < 0$, $v_p > 1$). For calculation of mean values, these pixels were set to zero or 1, respectively.

Immunohistochemistry

Experimental details of the immunohistochemistry study are available in the Supplementary Data.

Statistical analysis

Values are presented as mean ± standard error, unless otherwise stated. All statistical analysis was performed with GraphPad Prism 5. The goodness of fit of the concentration curve by the mono- or bi-exponential model was assessed using Pearson's correlation coefficient r. A one-way ANOVA test (Tukey's test) was used to compare absolute pharmacokinetic parameters of GdCAs. Unpaired two-sided *t*-tests (with Welch's correction, when unequal population variances) were used to compare mean changes between control and treated groups. *P*-values (two-tailed) <0.05(*) were considered as statistically significant.

RESULTS

Figure 1 (a–c) shows typical magnitude data from a time series of T_1-weighted images, measured in the mouse iliac artery/vein receiving gadoterate, p846 and p792, respectively. The dip in arterial signal makes it impossible to quantify the AIF with magnitude imaging. As shown on Figure 1(d—f), with phase imaging, a clear positive bolus peak is observed after injection of gadoterate, p846 and p792, respectively. For gadoterate and p846, in some mice, there is an apparent drop below 0 on late points of the curve, as shown on Figure 1(d–e). The concentration curve in plasma was correctly fitted by the bi-exponential function for gadoterate and p846 [r (±SD) of 0.82 (±0.09) and 0.82 (±0.11) for gadoterate and p846; $^{***}p < 0.0001$] and by the mono-exponential function for p792 [$r = 0.85$ (±0.09); $^{***}p < 0.0001$]. It should be noted that, for some mice, the upslope of the first pass peak was not accurately fitted. The peak concentration in plasma measured from the mean maximum $\Delta\Phi$ of untreated mice is 4.7 ± 1.9 mM, 4.2 ± 2.2 mM and 5.5 ± 1.4 mM for gadoterate (0.29 mmol Gd/kg), p846 (0.10 mmol Gd/kg) and p792 (0.15 mmol Gd/kg), respectively (mean ± SD).

Figure 2 illustrates the enhancement curves obtained in tumors after GdCA injection for control and CA4-treated groups using the three different GdCAs. For control groups, the GdCA administration resulted in a clear enhancement in the tumor. We observed a rapid and large enhancement for gadoterate (Fig. 2a). For p846 (Fig. 2b), the enhancement was also characterized by an early rise but smaller in amplitude. For the highest MW GdCA p792 (Fig. 2 c), the enhancement was delayed, with a maximum amplitude occurring around 1000 s after the bolus. In CA4-treated mice, the amplitude in the signal intensity enhancement was smaller compared with control mice and the washout was also slower, and this was true for each GdCA (Fig. 2). The signal-to-noise ratio (SNR) was calculated for the untreated group of each contrast agent as follows: $SNR = S_t/SD_n$ where S_t is the mean signal intensity of the tumour ROI and SD_n the standard deviation of the noise (31). SNR values of the first set of 400 scans were 85.1 ± 2.8, 59.1 ± 4.6, 58.9 ± 5.2 for gadoterate, p846 and p792, respectively (average of untreated mice). The second slower part of the acquisition (300 scans every 10.1 s) had a ~ two-fold increase of the SNR (147.7 ± 13.0, 110.2 ± 11.3 and 105.7 ± 25.65 for gadoterate, p846 and p792).

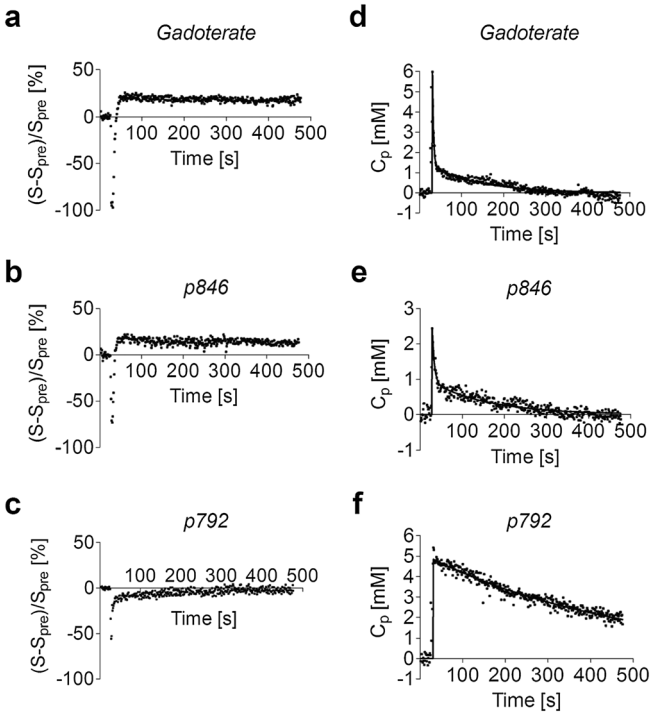

Figure 1. (a–c) Typical input function acquired in iliac artery/vein of mice with magnitude imaging using gadoterate (a), p846 (b) and p792 (c). Note the negative dip in arterial signal which makes it impossible to quantify the arterial input function (AIF) with magnitude imaging; (d–f) Typical time course of concentration in plasma (C_p) obtained with phase imaging for gadoterate (d), p846 (e) and p792 (f). Experimental data represented by (•) were modeled with a mono- or a bi-exponential fitting (–).

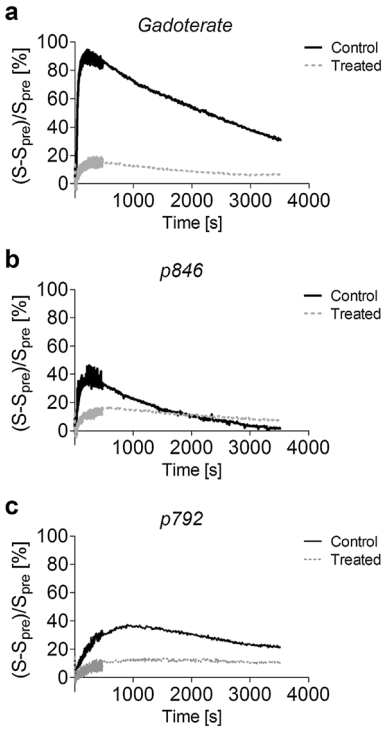

Figure 2. Typical signal enhancement in % observed in transplantable liver tumor (TLT) hepatocarcinoma for the control (dark solid line) and treated (gray dotted line) group of gadoterate (a), p846 (b), p792 (c). A smaller enhancement and a slower washout were observed for each treated group compared with the control group.

Figure 3 shows the pharmacokinetic parameters K^{trans} and v_p determined for each GdCA in the TLT tumors of untreated mice. Mean K^{trans} values were 0.58 (±0.12), 0.41 (±0.11) and 0.030 (±0.004) min^{-1} for gadoterate, p846 and p792, respectively (Fig. 3a). A significant difference was observed between K^{trans} obtained with p792 compared with K^{trans} obtained with gadoterate ($^{**}p < 0.01$) or p846 ($^{*}p < 0.05$). A decrease of K^{trans} values was observed as the MW of the GdCA increases. The fractional plasma volume v_p showed the same trends with mean values of 0.33 (±0.13), 0.16 (±0.06) and 0.014 (±0.003) for gadoterate, p846 and p792, respectively, with no statistically significant differences between contrast agents (Fig. 3b).

In Figure 4, K^{trans} and v_p are expressed as a percentage of baseline for control and CA4-treated groups. A significant decrease of K^{trans} was observed in CA4-treated groups compared with the control groups (Fig. 4a) for each GdCA ($^{*}p < 0.05$). Regarding the fractional plasma volume v_p, a decrease was

NMR IN BIOMEDICINE

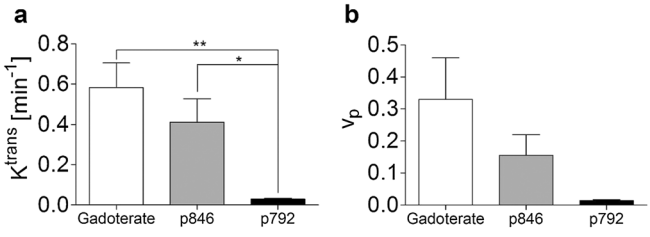

Figure 3. Absolute values of pharmacokinetic parameters K^{trans} (a) and v_p (b) determined with gadoterate, p846 and p792 for untreated tumors. A significant difference was observed between K^{trans} obtained with p792 compared with K^{trans} obtained with gadoterate (**$p < 0.01$) or p846 (*$p < 0.05$). Concerning v_p, no statistically significant differences was observed between contrast agents. An inverse relationship between MW of contrast agent and K^{trans} and v_p values was observed.

observed for all GdCAs, but this trend was not statistically significant (Fig. 4b). CA4 treatment caused a mean K^{trans} decrease of 77.6%, 79.6% and 55.8% for gadoterate, p846 and p792, respectively (Fig. 4a). Thus, the extent of the decrease was less marked with p792, although the difference was not statistically significant compared with the two other agents. The same trend was observed for v_p changes induced by CA4 with the lower reduction observed for p792 (42.0% of decline; $p = 0.21$), followed by gadoterate (67.8%; $p = 0.16$) and p846 (90.6%; $p = 0.08$) (Fig. 4b). Immunohistochemistry revealed a decrease of 71.4% of the vascular perfusion marker Hoechst 33342 (Fig. 4c) in the treated group compared with the control group. No change was observed in vascular density assessed by CD31 antibody after treatment (Fig. 4d).

Figure 5 shows a typical K^{trans} map obtained from an untreated and a treated mouse with each contrast agent (Fig. 5a). Ktrans values were lower in treated compared with untreated mice for each GdCA. A higher proportion of non-perfused pixels ($K^{trans} < 0$) was also observed for treated tumors, in particular for p846 and p792. Illustrative pictures of tumor sections stained with CD31 antibody and Hoechst 33342 are shown for an untreated (Fig. 5b) and a treated mouse (Fig. 5c). Treated tumors showed less perfused vessels (assessed with Hoechst 33342, administered 2 min before sacrifice) compared with untreated tumors. Concerning the vascular density (assessed with CD31 antibody), no difference between treated and untreated tumors was observed.

T_1-weighted images from iliac arteries/veins before, 28 s after and ~90 s after the GdCA injection are shown on Fig. S1, added in Supplementary material. The susceptibility effects are visible as a darkening of the iliac arteries/veins just after the GdCA injection, corresponding to the dip in magnitude signal.

Examples of fitting of pixel tissue concentration curves for an untreated mouse of each contrast agent are shown on Fig. S2, added as Supplementary material.

DISCUSSION

Ultra-high-field MRI provides greater SNR and consequently a possible reduction of acquisition time for higher-resolution scanning. Therefore, we can obtain high DCE-MRI temporal resolution while maintaining adequate spatial resolution, providing a powerful tool to monitor the early effects of VDAs in mouse tumors. In this study, we demonstrated the feasibility of DCE-MRI at 11.7 T to assess tumor hemodynamics of mice. The method allowed monitoring of an early tumor response to an acute treatment of CA4 (100 mg/kg), by determining pharmacokinetic parameters K^{trans} and v_p of untreated and treated tumors with the ETM. The comparison of the value of three GdCAs of increasing MW (Gadoterate, p846 and p792) in the monitoring of CA4 activity was also performed.

Feasibility of DCE-MRI at 11.7 T

For quantitative DCE-MRI, the AIF, defined as the time-dependent GdCA concentration in the vessels feeding the tumor, should be

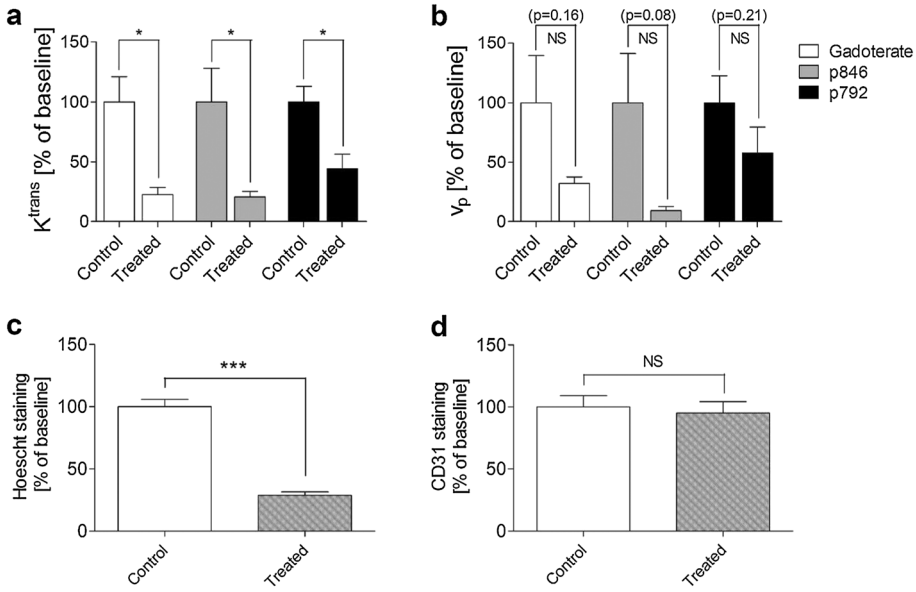

Figure 4. Relative changes of K^{trans} (a) and v_p (b) between untreated and treated tumors for gadoterate (white bars), p846 (grey bars) and p792 (black bars). A smaller decline of K^{trans} and v_p was observed for the highest MW GdCA p792 compared with gadoterate and p846, although this was not statistically significant. Relative decreases of Hoechst (c) and CD31 (d) staining between untreated and treated tumors. A significant decrease of perfusion marker was observed in the treated group compared with the control group. No difference was observed in vascular density assessed by CD31.

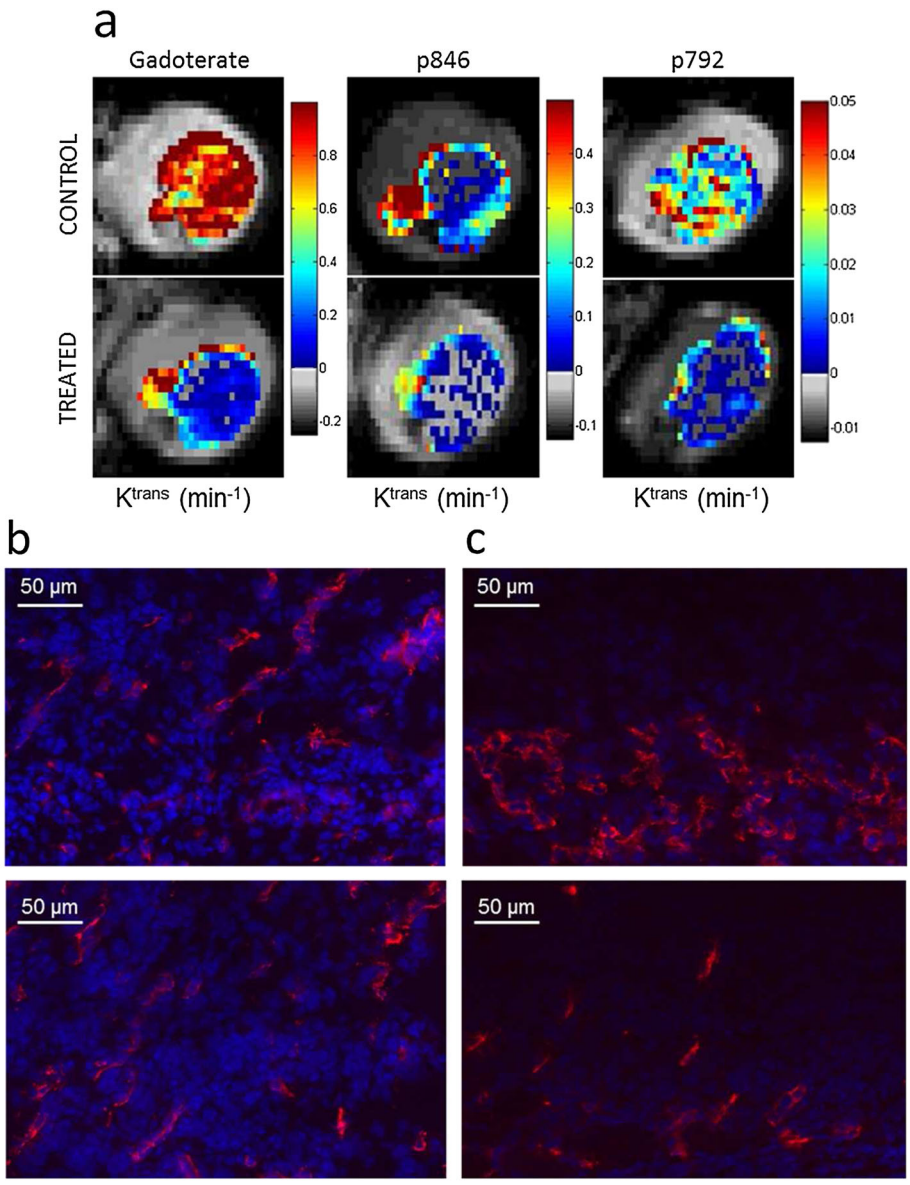

Figure 5. (a) Illustration of a typical K^{trans} map obtained from an untreated and a treated mouse with each GdCa. K^{trans} values were lower in treated mice compared with untreated mice. A higher proportion of non-perfused pixels ($K^{trans} < 0$) was also observed in treated mice. (b–c) Representative pictures of tumor sections from an untreated mouse (b) and a treated mouse (c) stained with CD31 antibody for endothelial cells (red). The perfusion marker Hoechst 33342 (blue) was injected 2 min before sacrifice. The CA4 effects were clearly visualized by a less presence of perfused vessels in treated tumors compared with untreated tumors. No difference was observed for vascular density.

measured accurately. Measurement of the AIF is quite challenging at 11.7 T due to increased T_2* susceptibility effects, particularly in blood vessels immediately after the bolus contrast injection, where the GdCA concentration is high. Consequently, with magnitude imaging, a signal drop in the arteries was observed after the administration of each GdCA (Fig. 1 and Fig. S1). Recently, we suggested the use of phase imaging as an alternative to magnitude imaging for AIF measurements when using gadoterate at 11.7 T (12). In the present study, we extended this method to the two other GdCAs, namely p846 and p792. Using phase imaging, it was possible to measure the AIF from the iliac artery/vein (the distinction between artery and vein was not easily feasible). As shown in Fig. 1, we observed a bi-exponential profile similar to those previously described in mice for gadoterate (32) and for p846 (19). The mono-exponential decay observed for p792 is also consistent with results previously described (33). The C_p value obtained with gadoterate (4.7 ± 1.9 mM) is close to that reported by Vautier *et al.* (34) in the left ventricle of mice with a similar dose (3.4 ± 1.1 mM; 0.3 mmol/kg). Moreover, Heilmann *et al.* reported a peak AIF concentration of 8.0 ± 2.7 mM using a ~ two-fold dose of gadoterate in the heart of nude mice (0.6 mmol/kg). The mean C_p value determined with the contrast agent p846 (4.2 ± 2.2 mM) is slightly higher than that obtained by Loveless *et al.* (~1.5 mM which was obtained with the half of our dose). The same observation can be made for p792 (5.5 ± 1.4 mM) compared with the Bradley *et al.* study [peak concentration of 1.15 ± 0.18 mM in the left ventricle using a three-fold-lower dose (35)].

Although in agreement with literature data, the mean peak plasma concentration determined for gadoterate is smaller than

that previously found in our lab in the same mouse strain (4.7 ± 1.9 mM versus 8.0 ± 0.6 mM) (12). We also observed a larger standard deviation. It confirmed the difficulties of AIF measurement with phase imaging in iliac artery owing to phase's angle dependence. The iliac artery is oriented at about 30° with respect to B0 demanding special care of the position of the mice in the magnet. Indeed, the inter-individual variation in iliac artery angulation was not taken into account for the C_p calculation. Moreover, a model taking into account geometrical information and shape factors should be used to deal with the curvature and bifurcations of the artery (36).

Moreover, for gadoterate and p846, in some mice, there is an apparent drop below 0 on late points of the C_p curve (Fig. 1d–e). This could be due to a difficult correction of the background phase for the AIF for these GdCAs. Indeed, in our recent study on AIF measurement using gadoterate (12), and as previously outlined by Garpebring (37), we conjectured that the presence of low concentrations of GdCA in the background ROI selected could lead to an excessive correction of the phase drift.

Comparison of K^{trans} and v_p obtained in TLT tumors with the three contrast agents

Using individual AIFs, the tissue concentration curves were fitted with the ETM to generate K^{trans} and v_p values. K^{trans} represents the rate of transfer of the GdCA from the blood to the EES and depends on the balance between capillary permeability and blood flow in the tumor (30). If the delivery of the GdCA to a tissue is insufficient (flow-limited cases or where vascular permeability is greater than inflow), perfusion dominates the GdCA behavior, and K^{trans} is equal to the blood plasma flow per unit volume of tissue (F_p). In contrast, when tissue contrast delivery is ample (permeability-limited cases), K^{trans} is equivalent to the product of the permeability and surface area [permeability surface area product (PS)] (2,30,38). In tumors, a mixed flow- and PS-limited case is often considered (30). However, several groups have reported that K^{trans} measured with low-MW GdCAs is dominated by perfusion whereas PS is the dominant factor when K^{trans} is measured with high-MW GdCAs (15,16,33,39). Indeed, the MW of the GdCA affects its permeability across the capillary membrane, explaining the inverse relationship observed between MW of the GdCAs and K^{trans} values (Fig. 3a). The same observation was made by Delrue *et al*. in a pancreatic tumor model (39). Gadoterate, the smallest GdCA tested in the present study, can diffuse from the intravascular space into the EES of normal tissues (with the exception of the brain) but can diffuse more easily into the EES of tumors (due to greater permeability). P846 and p792 are considered blood pool agents as they remain within the intravascular compartment for a longer period (40). p846 (3.5 kDa) can diffuse through the endothelium but at a slower rate than gadoterate. The highest MW GdCA p792 (6.5 kDa) has limited diffusion across the normal vascular endothelium and thus a preferential accumulation within the tumor owing to the increased capillary permeability (23). Referring to literature, our mean K^{trans} values determined with gadoterate and p846 turned out to be higher than those reported by Delrue *et al*. (39) (0.17 and 0.074 min^{-1}, respectively) in mouse pancreatic tumors. For p792, there is no significant difference with the Delrue *et al*. (0.016 min^{-1}) and Weidensteiner *et al*. (averaged median K^{trans} of 0.015 min^{-1}) studies (33). Although these studies used ETM, it is hard to compare with our work due to the different ways the AIF was measured.

The parameter v_p represents the blood plasma volume per unit volume of tissue (30) (or 'fractional plasma volume'). We observed an inverse relationship between the MW of the GdCAs and the v_p values in untreated tumors (Fig. 3b). Several papers in the literature have shown that low MW GdCAs are less adapted to enable accurate estimation of blood volume owing to their rapid extravasation rate into the EES, leading to an overestimation of v_p values (3,15,41,42). The high leakage rate renders the fitting more difficult as the vascular and leakage phase cannot be separated (33). It can in part explain the high values found for v_p determined with gadoterate (560 Da; $v_p = 0.33 \pm 0.13$) and p846 (3.5 kDa; $v_p = 0.16 \pm 0.06$). Indeed, microvascular density assessed by CD31 staining of endothelial cells has revealed a vascular density of 3.3 ± 0.9% in TLT hepatocarcinoma. De Lussanet *et al*. reported a sharp decrease in v_p values determined with GdCAs of 3.0- and 12-kDa, suggesting a possible threshold for the intravascular compartmentalization of the GdCA, further allowing a better estimation of the fractional plasma volume. This is consistent with the large v_p difference we observed between p846 (3.5 kDa; $v_p = 0.16 \pm 0.06$) and p792 (6.5 kDa; $v_p = 0.014 \pm 0.003$). The low values we found for v_p determined with p792 are consistent with the weak perfusion of the TLT hepatocarcinoma model (43) and are similar to the vascular density determined in the immunochemistry study (3.3%). Moreover, a study of Turetschek *et al*. in experimental breast tumors (44) reported that fractional plasma volumes determined using p792 were not significantly different than those determined using albumin-(Gd-DTPA)[30], a GdCA which has proven to be successful in the accurate estimation of tissue plasma volume (45).

Another explanation of these high gadoterate and p846 v_p values could arise from the pharmacokinetic model used. Sourbron and Buckley reported that this model is valid only in highly perfused tissues and in weakly vascularized tissues with a well-mixed interstitium (27). Moreover, they reported that even in the case of a correct fitting of tissue concentration curves, the measured parameter values could be different from the actual values (46). In our study, the fitting of concentration-time curves was not perfect for some pixels of the tumor (Fig. S2). The vascular volume is considered as a shunt in the ETM (13). A four parameter model in which plasma and interstitial volumes are modeled as both compartments should be used as comparison, e.g. the two-compartment exchange model (2CXM). Actually, the ETM is a simplification of the 2CXM, by assuming that the mean plasma transit time is negligible (47).

Value of the 3 GdCAs to monitor the effect of CA4

Whatever the GdCA used, DCE-MRI allowed the detection of early effects of an acute CA4 treatment on tumor vasculature, as shown in Figure 2. Enhancement curves displayed a smaller enhancement and a slower washout in each CA4-treated group compared with untreated groups. As shown in Figure 4, the pharmacokinetic modeling confirmed the profound changes induced by CA4 on tumor hemodynamics, as reflected by the significant decrease of K^{trans} observed between control and treated groups for each GdCA. Although caution should be taken in the physiological interpretation of K^{trans}, the K^{trans} changes observed in our study are probably related to tumor blood flow changes, as supported by the immunohistochemistry experiment. Indeed, the decrease of K^{trans} of gadoterate (77.6%) and p846 (79.6%) observed in treated groups compared with control

groups are closed to the decline of perfusion marker Hoechst 33342 (71.4%) observed in treated group of immunohistochemistry study. The early reduction in blood flow induced by CA4 has been observed in several studies with radioactive tracers (48) and Hoechst 33342 (49). In addition, Maxwell *et al.* (10) reported a strong correlation between tumor blood flow determined by radiolabeled iodoantipyrine uptake and mean K^{trans} values determined with the small MW contrast agent Gd-DTPA in both untreated and treated rat P22 sarcomas. CA4 is also known to induce a decrease in blood flow concomitant with a permeability increase (5), so that treatment could cause a shift to a flow-limited situation (10,50). The smaller decline we observed for the highest MW GdCA p792 compared with gadoterate and p846 (Fig. 4) may be as a result of the early increase in permeability induced by CA4 treatment. This is consistent with the larger importance of permeability to K^{trans} values for this higher MW agent compared with smaller MW GdCAs such as gadoterate and p846. A model allowing separate measures of F_p and PS, such as the 2CXM, is needed to further distinct permeability from blood flow changes after CA4 treatment.

Concerning the impact of CA4 on the fractional plasma volume v_p, we observed a trend of decrease for the three GdCAs although it was not statistically significant. The immunohistochemistry study showed that 2 h after treatment, no effect of vascular density is shown on TLT model. This confirmed that due to the high leakage rate of gadoterate, p846 and to a smaller extent of p792, the observed decrease of v_p is confounded by changes in delivery (perfusion).

Possible limitations of the present study

Our study has potential shortcomings. First of all, susceptibility effects are increased at high field and the longitudinal relaxivity r_1 is decreased for these GdCAs (Table 1). The decrease in r_1 was not dramatic for gadoterate, which shows a ~25% decrease at 11.7 T compared with 1.5 T. However, for the case of p846 and p792, r_1 relaxivities were decreased by a factor of 5 and 9, respectively, at 11.7 T compared with 1.5 T. Consequently, we used higher doses than those commonly used at clinical fields, which could lead to further accentuated T_2* susceptibility effects. The determination of the AIF using phase imaging was not problematic as a linear relationship between phase and gadolinium concentration has been demonstrated, with no saturation effect (12). However, in tumors, we assumed that susceptibility effects are negligible because the concentration of the GdCA is much lower than in blood vessels and, moreover, the extravasation of the GdCA reduces the susceptibility contrast. Nevertheless, a correction for T_2* dephasing should be included, as outlined by Ewing and Bagher-Ebadian who showed that T_2* dephasing is a major source of bias in the estimate of CA concentration-time curves at 7 T in brain tumors (51). Moreover, due to these higher doses, a possible saturation of the signal in tumor cannot be fully excluded.

Concerning AIF data analysis, in general, the use of automatic algorithms instead of manual post-processing (for pixel selection, unwrapping and phase drift correction) could improve the reliability of the results. In particular, an algorithm partitioning the background region based on signal intensity to detect regions less affected by the CA accumulation, as presented by Garperbring *et al.* (37), could be useful to avoid excessive correction of phase drift. The large standard errors observed on vascular volume fraction measured using gadoterate and p846 could be explained in part by this difficult correction of background phase. The smaller error observed for v_p determined with p792 is consistent with its preferential accumulation in tumor compared with other tissues (in which the background ROI was selected). In addition, in some mice, the bi-exponential model failed to fit the upslope data points of the AIF raw data. As demonstrated by McGrath *et al.* (52), the poor fitting by the bi-exponential model for points on the upslope of the first pass peak is not very critical to the estimation of K^{trans} but can affect v_p. It should also be noted that AIF parameters were extracted from the first 400 scans and not from the 1 h of acquisition. The estimation of clearance parameters might be affected and their estimation could be improved by acquiring AIF parameters on all sampling data. However, in this case, the phase drift could be further amplified and consequently more difficult to correct.

As previously explained, the pharmacokinetic model used could, in part, explain the questionable results concerning v_p. A four-parameter model, as 2CXM, could provide more accurate values of v_p by taking into consideration the mean plasma transit time. Such a model could also provide separate estimation of F_p and PS potentially visualizing permeability changes induced by treatment (e.g. masked by the blood flow shutdown). Nevertheless, ideally one should determine which of the two models fits the data better. Indeed, Larsson *et al.* have shown that the 2CXM failed to fit the data when all four parameters are free (53). One solution could be to fix the value of at least one parameter while varying the other three. However, this approach could bias the final results (51).

Another assumption of the ETM is that the tracer is well mixed throughout the compartments. This assumption is not strictly true over the first pass of the GdCA, in regions where the GdCA has no access (brain and testis) and in tumor regions with high interstitial fluid pressure. It must also be kept in mind that the model should be adapted to the pharmacokinetic properties of the GdCA, as outlined by Jaspers *et al.* (54). Moreover, the transmembrane water exchange has not been considered, which could lead to errors in the calculation of the tissue GdCA concentration (2). The shutter speed model (55) might be able to take into account this component.

Finally, for calculation of mean values, individual pixel values of K^{trans} and v_p were forced into the range of 0 to 1 to avoid outliers affecting the mean. Negative values were set to 0, and high values (>1) were set to 1. We verified that this forcing did not induce significant bias in the data analysis. The relative changes observed between control and treated groups were comparable when high value forcing was not applied (93.3, 90.0 and 55.8% of decline for K^{trans} determined with gadoterate, p846 and p792, respectively, and 82.1%, 90.8% and 42.0% of decline for v_p determined with gadoterate, p846 and p792).

CONCLUSIONS

DCE-MRI at 11.7 T is feasible to assess tumor hemodynamics of mice, in spite of the increase in susceptibility effects and decrease in r1 relaxivity of GdCAs at high field. With regard to K^{trans}, the three GdCAs (gadoterate, p846, and p792) all worked well for detecting early vascular effects induced by CA4 in murine tumors. The observed K^{trans} declines are likely related to blood flow shutdown, as revealed by the separate immunochemistry study. The smaller decline we observed for the highest MW GdCA (p792) may be as a result of the early increase in permeability

induced by CA4 treatment. It suggests that smaller GdCAs should be more able to highlight the early blood flow shutdown induced by CA4 treatment, as their K^{trans} is less influenced by permeability. However, a pharmacokinetic model allowing separate measurement of perfusion and permeability changes after CA4 treatment is needed to corroborate this idea. Besides the pharmacokinetic modeling, other limitations in quantification of pharmacokinetic parameters exist in this study, such as non-correction of T_2* effects and non-optimization of phase drift correction for AIF measurement.

Acknowledgements

This study was supported by a grant from the Belgian Foundation against cancer, ARC 09/14-020, the Fonds Joseph Maisin and the FNRS. We thank Philippe Robert from Guerbet for providing the contrast agents. We thank R. N. Muller, S. Laurent and L. Vander Elst (University of Mons) for relaxivity measurement at 500 MHz.

REFERENCES

1. Padhani AR, Miles KA. Multiparametric imaging of tumor response to therapy. Radiology 2010; 256: 348–364.
2. Zweifel M, Padhani AR. Perfusion MRI in the early clinical development of antivascular drugs: decorations or decision making tools? Eur. J. Nucl. Med. Mol. Imaging 2010; 37(Suppl 1): S164–182.
3. Jaspers K, Aerts HJ, Leiner T, Oostendorp M, van Riel NA, Post MJ, Backes WH. Reliability of pharmacokinetic parameters: small vs. medium-sized contrast agents. Magn. Reson. Med. 2009; 62: 779–787.
4. O'Connor JP, Jackson A, Parker GJ, Roberts C, Jayson GC. Dynamic contrast-enhanced MRI in clinical trials of antivascular therapies. Nat. Rev. Clin. Oncol. 2012; 9: 167–177.
5. Tozer GM, Kanthou C, Baguley BC. Disrupting tumour blood vessels. Nat. Rev. Cancer 2005; 5: 423–435.
6. Tozer GM, Kanthou C, Parkins CS, Hill SA. The biology of the combretastatins as tumour vascular targeting agents. Int. J. Exp. Pathol. 2002; 83: 21–38.
7. Zweifel M, Jayson GC, Reed NS, Osborne R, Hassan B, Ledermann J, Shreeves G, Poupard L, Lu SP, Balkissoon J, Chaplin DJ, Rustin GJ. Phase II trial of combretastatin A4 phosphate, carboplatin, and paclitaxel in patients with platinum-resistant ovarian cancer. Ann. Oncol. 2011; 22: 2036–2041.
8. Nathan P, Zweifel M, Padhani AR, Koh DM, Ng M, Collins DJ, Harris A, Carden C, Smythe J, Fisher N, Taylor NJ, Stirling JJ, Lu SP, Leach MO, Rustin GJ, Judson I. Phase I trial of combretastatin A4 phosphate (CA4P) in combination with bevacizumab in patients with advanced cancer. Clin. Cancer Res. 2012; 18: 3428–3439.
9. Nielsen T, Murata R, Maxwell RJ, Stødkilde-Jørgensen H, Østergaard L, Ley CD, Kristjansen PEG, Horsman MR. Non-invasive imaging of combretastatin activity in two tumor models: Association with invasive estimates. Acta Oncol. 2010; 49: 906–913.
10. Maxwell RJ, Wilson J, Prise VE, Vojnovic B, Rustin GJ, Lodge MA, Tozer GM. Evaluation of the anti-vascular effects of combretastatin in rodent tumours by dynamic contrast enhanced MRI. NMR Biomed. 2002; 15: 89–98.
11. Caravan P, Farrar CT, Frullano L, Uppal R. Influence of molecular parameters and increasing magnetic field strength on relaxivity of gadolinium- and manganese-based T1 contrast agents. Contrast Media Mol. Imaging 2009; 4: 89–100.
12. Fruytier AC, Magat J, Colliez F, Jordan B, Cron G, Gallez B. Dynamic contrast-enhanced MRI in mice at high field: Estimation of the arterial input function can be achieved by phase imaging. Magn. Reson. Med. 2013. doi: 10.1002/mrm.24682. [Epub ahead of print].
13. Michoux N, Huwart L, Abarca-Quinones J, Dorvillius M, Annet L, Peeters F, Van Beers BE. Transvascular and interstitial transport in rat hepatocellular carcinomas: dynamic contrast-enhanced MRI assessment with low- and high-molecular weight agents. J. Magn. Reson. Imaging 2008; 28: 906–914.
14. Leach MO, Brindle KM, Evelhoch JL, Griffiths JR, Horsman MR, Jackson A, Jayson GC, Judson IR, Knopp MV, Maxwell RJ, McIntyre D, Padhani AR, Price P, Rathbone R, Rustin GJ, Tofts PS, Tozer GM, Vennart W, Waterton JC, Williams SR, Workman P. The assessment of antiangiogenic and antivascular therapies in early-stage clinical trials using magnetic resonance imaging: issues and recommendations. Br. J. Cancer 2005; 92: 1599–1610.
15. de Lussanet QG, Langereis S, Beets-Tan RG, van Genderen MH, Griffioen AW, van Engelshoven JM, Backes WH. Dynamic contrast-enhanced MR imaging kinetic parameters and molecular weight of dendritic contrast agents in tumor angiogenesis in mice. Radiology 2005; 235: 65–72.
16. Daldrup H, Shames DM, Wendland M, Okuhata Y, Link TM, Rosenau W, Lu Y, Brasch RC. Correlation of dynamic contrast-enhanced MR imaging with histologic tumor grade: comparison of macromolecular and small-molecular contrast media. AJR Am. J. Roentgenol. 1998; 171: 941–949.
17. Taper HS, Woolley GW, Teller MN, Lardis MP. A new transplantable mouse liver tumor of spontaneous origin. Cancer Res. 1966; 26: 143–148.
18. Grosios K, Holwell SE, McGown AT, Pettit GR, Bibby MC. In vivo and in vitro evaluation of combretastatin A-4 and its sodium phosphate prodrug. Br. J. Cancer 1999; 81: 1318–1327.
19. Loveless ME, Halliday J, Liess C, Xu L, Dortch RD, Whisenant J, Waterton JC, Gore JC, Yankeelov TE. A quantitative comparison of the influence of individual versus population-derived vascular input functions on dynamic contrast enhanced-MRI in small animals. Magn. Reson. Med. 2012; 67: 226–236.
20. Jacquier A, Bucknor M, Do L, Robert P, Corot C, Higgins CB, Saeed M. P846, a new gadolinium based low diffusion magnetic resonance contrast agent, in characterizing occlusive infarcts, reperfused ischemic myocardium and reperfused infarcts in rats. MAGMA 2008; 21: 207–218.
21. Port M, Corot C, Rousseaux O, Raynal I, Devoldere L, Idee JM, Dencausse A, Le Greneur S, Simonot C, Meyer D. P792: a rapid clearance blood pool agent for magnetic resonance imaging: preliminary results. MAGMA 2001; 12: 121–127.
22. Gaillard S, Kubiak C, Stolz C, Bonnemain B, Chassard D. Safety and pharmacokinetics of p792, a new blood-pool agent: results of clinical testing in nonpatient volunteers. Invest. Radiol. 2002; 37: 161–166.
23. Bourasset F, Dencausse A, Bourrinet P, Ducret M, Corot C. Comparison of plasma and peritoneal concentrations of various categories of MRI blood pool agents in a murine experimental pharmacokinetic model. MAGMA 2001; 12: 82–87.
24. Lemasson B, Christen T, Tizon X, Farion R, Fondraz N, Provent P, Segebarth C, Barbier EL, Genne P, Duchamp O, Remy C. Assessment of multiparametric MRI in a human glioma model to monitor cytotoxic and anti-angiogenic drug effects. NMR Biomed. 2011; 24: 473–482.
25. Tofts PS, Kermode AG. Measurement of the blood–brain barrier permeability and leakage space using dynamic MR imaging. 1. Fundamental concepts. Magn. Reson. Med. 1991; 17: 357–367.
26. Baudelet C, Ansiaux R, Jordan BF, Havaux X, Macq B, Gallez B. Physiological noise in murine solid tumours using T2*-weighted gradient-echo imaging: a marker of tumour acute hypoxia? Phys. Med. Biol. 2004; 49: 3389–3411.
27. Sourbron SP, Buckley DL. Classic models for dynamic contrast-enhanced MRI. NMR Biomed. 2013; 26: 1004–1027
28. Buckley DL, Parker GJM. Measuring contrast agent concentration in T1-weighted dynamic contrast-enhanced MRI. In: *Dynamic Contrast-Enhanced Magnetic Resonance Imaging in Oncology* (Jackson A, Buckley DL, Parker GJM eds). Springer: Berlin, 2005, 69–79.
29. Heilmann M, Kiessling F, Enderlin M, Schad LR. Determination of pharmacokinetic parameters in DCE MRI: Consequence of nonlinearity between contrast agent concentration and signal intensity. Invest. Radiol. 2006; 41: 536–543.
30. Tofts PS, Brix G, Buckley DL, Evelhoch JL, Henderson E, Knopp MV, Larsson HB, Lee TY, Mayr NA, Parker GJ, Port RE, Taylor J, Weisskoff RM. Estimating kinetic parameters from dynamic contrast-enhanced T(1)-weighted MRI of a diffusable tracer: standardized quantities and symbols. J. Magn. Reson. Imaging 1999; 10: 223–232.
31. Dietrich O, Raya JG, Reeder SB, Reiser MF, Schoenberg SO. Measurement of signal-to-noise ratios in MR images: influence of multichannel coils, parallel imaging, and reconstruction filters. J. Magn. Reson. Imaging 2007; 26: 375–385.
32. Heilmann M, Walczak C, Vautier J, Dimicoli JL, Thomas CD, Lupu M, Mispelter J, Volk A. Simultaneous dynamic T1 and T2* measurement for AIF assessment combined with DCE MRI in a mouse tumor model. MAGMA 2007; 20: 193–203.

33. Weidensteiner C, Rausch M, McSheehy PM, Allegrini PR. Quantitative dynamic contrast-enhanced MRI in tumor-bearing rats and mice with inversion recovery TrueFISP and two contrast agents at 4.7 T. J. Magn. Reson. Imaging 2006; 24: 646–656.
34. Vautier J, El Tannir El Tayara N, Walczak C, Mispelter J, Volk A. Radial multigradient-echo DCE-MRI for 3D K(trans) mapping with individual arterial input function measurement in mouse tumor models. Magn. Reson. Med. 2013; 70: 823–828.
35. Bradley DP, Tessier JL, Checkley D, Kuribayashi H, Waterton JC, Kendrew J, Wedge SR. Effects of AZD2171 and vandetanib (ZD6474, Zactima) on haemodynamic variables in an SW620 human colon tumour model: an investigation using dynamic contrast-enhanced MRI and the rapid clearance blood pool contrast agent, P792 (gadomelitol). NMR Biomed. 2008; 21: 42–52.
36. de Rochefort L, Nguyen T, Brown R, Spincemaille P, Choi G, Weinsaft J, Prince MR, Wang Y. In vivo quantification of contrast agent concentration using the induced magnetic field for time-resolved arterial input function measurement with MRI. Med. Phys. 2008; 35: 5328.
37. Garpebring A, Wirestam R, Yu J, Asklund T, Karlsson M. Phase-based arterial input functions in humans applied to dynamic contrast-enhanced MRI: potential usefulness and limitations. MAGMA 2011; 24: 233–245.
38. O'Connor JPB, Jackson A, Parker GJM, Jayson GC. DCE-MRI biomarkers in the clinical evaluation of antiangiogenic and vascular disrupting agents. Br. J. Cancer 2007; 96: 189–195.
39. Delrue LJ, Casneuf V, Van Damme N, Blanckaert P, Peeters M, Ceelen WP, Duyck PCO. Assessment of neovascular permeability in a pancreatic tumor model using dynamic contrast-enhanced (DCE) MRI with contrast agents of different molecular weights. MAGMA 2011; 24: 225–232.
40. Corot C, Port M, Raynal I, Dencausse A, Schaefer M, Rousseaux O, Simonot C, Devoldere L, Lin J, Foulon M, Bourrinet P, Bonnemain B, Meyer D. Physical, chemical, and biological evaluations of P760: a new gadolinium complex characterized by a low rate of interstitial diffusion. J. Magn. Reson. Imaging 2000; 11: 182–191.
41. Cheng HL, Wallis C, Shou Z, Farhat WA. Quantifying angiogenesis in VEGF-enhanced tissue-engineered bladder constructs by dynamic contrast-enhanced MRI using contrast agents of different molecular weights. J. Magn. Reson. Imaging 2007; 25: 137–145.
42. Feng Y, Jeong EK, Mohs AM, Emerson L, Lu ZR. Characterization of tumor angiogenesis with dynamic contrast-enhanced MRI and biodegradable macromolecular contrast agents in mice. Magn. Reson. Med. 2008; 60: 1347–1352.
43. Cron GO, Beghein N, Ansiaux R, Martinive P, Feron O, Gallez B. 19 F NMR in vivo spectroscopy reflects the effectiveness of perfusion-enhancing vascular modifiers for improving gemcitabine chemotherapy. Magn. Reson. Med. 2008; 59: 19–27.
44. Turetschek K, Floyd E, Shames DM, Roberts TP, Preda A, Novikov V, Corot C, Carter WO, Brasch RC. Assessment of a rapid clearance blood pool MR contrast medium (P792) for assays of microvascular characteristics in experimental breast tumors with correlations to histopathology. Magn. Reson. Med. 2001; 45: 880–886.
45. Kuwatsuru R, Shames DM, Muhler A, Mintorovitch J, Vexler V, Mann JS, Cohn F, Price D, Huberty J, Brasch RC. Quantification of tissue plasma volume in the rat by contrast-enhanced magnetic resonance imaging. Magn. Reson. Med. 1993; 30: 76–81.
46. Sourbron SP, Buckley DL. On the scope and interpretation of the Tofts models for DCE-MRI. Magn. Reson. Med. 2011; 66: 735–745.
47. Luypaert R, Sourbron S, de Mey J. Validity of perfusion parameters obtained using the modified Tofts model: a simulation study. Magn. Reson. Med. 2011; 65: 1491–1497.
48. Tozer GM, Prise VE, Wilson J, Locke RJ, Vojnovic B, Stratford MR, Dennis MF, Chaplin DJ. Combretastatin A-4 phosphate as a tumor vascular-targeting agent: early effects in tumors and normal tissues. Cancer Res. 1999; 59: 1626–1634.
49. Zhao D, Richer E, Antich PP, Mason RP. Antivascular effects of combretastatin A4 phosphate in breast cancer xenograft assessed using dynamic bioluminescence imaging and confirmed by MRI. FASEB J. 2008; 22: 2445–2451.
50. Galbraith SM, Maxwell RJ, Lodge MA, Tozer GM, Wilson J, Taylor NJ, Stirling JJ, Sena L, Padhani AR, Rustin GJ. Combretastatin A4 phosphate has tumor antivascular activity in rat and man as demonstrated by dynamic magnetic resonance imaging. J. Clin. Oncol. 2003; 21: 2831–2842.
51. Ewing JR, Bagher-Ebadian H. Model selection in measures of vascular parameters using dynamic contrast-enhanced MRI: experimental and clinical applications. NMR Biomed. 2013; 26: 1028–1041.
52. McGrath DM, Bradley DP, Tessier JL, Lacey T, Taylor CJ, Parker GJ. Comparison of model-based arterial input functions for dynamic contrast-enhanced MRI in tumor bearing rats. Magn. Reson. Med. 2009; 61: 1173–1184.
53. Larsson HB, Courivaud F, Rostrup E, Hansen AE. Measurement of brain perfusion, blood volume, and blood–brain barrier permeability, using dynamic contrast-enhanced T(1)-weighted MRI at 3 tesla. Magn. Reson. Med. 2009; 62: 1270–1281.
54. Jaspers K, Leiner T, Dijkstra P, Oostendorp M, van Golde JM, Post MJ, Backes WH. Optimized pharmacokinetic modeling for the detection of perfusion differences in skeletal muscle with DCE-MRI: Effect of contrast agent size. Med. Phys. 2010; 37: 5746.
55. Li X, Huang W, Yankeelov TE, Tudorica A, Rooney WD, Springer CS, Jr. Shutter-speed analysis of contrast reagent bolus-tracking data: Preliminary observations in benign and malignant breast disease. Magn. Reson. Med. 2005; 53: 724–729.

SUPPORTING INFORMATION

Additional supporting information maybe found in the online version of this article at the publisher's web site.